Articles

XAFS Study of Gadolinium and Samarium Bisporphyrinate Complexes

Jean-Hugues Agondanou,[†] Georgios A. Spyroulias,[‡] Juris Purans,[†,§] Georgios Tsikalas,[‡] Charles Souleau,[†] Athanassios G. Coutsolelos,*[,‡] and Simone Bénazeth*[,†,||]

Laboratoire de Chimie Physique Minérale et Bioinorganique, EA401, UFR Pharmacie, Université Paris XI, 92296 Paris, France, Laboratory of Bioinorganic Coordination Chemistry, Department of Chemistry, University of Crete, P.O. Box 1470, 714 09 Heraklion, Crete, Greece, Laboratoire de biomathématiques, Faculté de pharmacie Université Paris V, 75006 Paris, France, LURE, Bat 209D Centre Universitaire Paris XI, 91405 Orsay, France, and Institute of Solid State Physics, University of Latvia-Kengaraga 8, 1063 Riga, Latvia

Received April 11, 2000

The comparative X-ray absorption spectroscopy study of gadolinium and samarium bisporphyrinate complexes represented by the formulas $Gd^{III}H(oep)(tpp)$, $Gd^{III}(oep)_2$, $Gd^{III}H(tpp)_2$ and $Sm^{III}H(oep)(tpp)$, $Sm^{III}(oep)_2$, $Sm^{III}H(tpp)_2$ is reported. The XAFS spectra are recorded on the LURE-DCI storage ring (Orsay, France) in transmission mode on the microcrystalline samples at the Gd and Sm L_3 edges. The local environment for Ln^{3+} ions has been reconstructed applying one-shell and two-shell XAFS analysis procedures. The protonated and nonprotonated bisporphyrinate complexes present different XAFS features. After our analysis on the title derivatives, the gadolinium ion (at 80 K) is found to be bonded: (i) to eight nitrogen atoms at R(Gd−N) 2.50 Å, for $Gd^{III}(oep)_2$ [Debye−Waller (DW) factor 0.004 Å^2]; (ii) to seven nitrogen atoms at R(Gd−N) 2.49 Å, for $Gd^{III}H(oep)(tpp)$ [DW factor 0.005 Å^2] and one nitrogen at long distance; and (iii) to six nitrogen atoms at R(Gd−N) 2.50 Å [DW factor 0.006 Å^2] and two nitrogen atoms at long distance for $Gd^{III}H(tpp)_2$. A similar coordination sphere has been detected for the corresponding Sm derivatives. So, the samarium ion (at room temperature) is bonded: (i) to eight nitrogen atoms at R(Sm−N) 2.53 Å, for $Sm^{III}(oep)_2$ [DW factor 0.006 Å^2]; (ii) to seven nitrogen atoms at R(Sm−N) 2.53 Å, for $Sm^{III}H(oep)(tpp)$ [DW factor 0.006 Å^2] and one nitrogen at long distance; and (iii) to six nitrogen atoms at R(Sm−N) 2.50 Å, for $Sm^{III}H(tpp)_2$ [DW factor 0.006 Å^2] and two nitrogen atoms at long distance. As far as concerns $Ln^{III}(oep)_2$ complexes, the increase of Ln−N distance in the series $Gd^{3+} < Eu^{3+} < Sm^{3+}$ reflects an increase in the ionic radii, which are in good agreement with previously published XRD data on $Eu^{III}(oep)_2$. Moreover, the protonated $Ln^{III}H(oep)(tpp)$ and $Ln^{III}H(tpp)_2$ complexes possess systematically shorter distances of about 0.02 Å between the XAFS and XRD data. This difference is attributed to the asymmetry of the distribution concerning Ln−N distances.

Introduction

The concept that there exist some structural and electronical similarities between the bacterial photosynthetic reactional center and the porphyrin sandwich-like complexes[1−5] gave rise to the synthesis of many lanthanide, actinide, Zr, and Hf porphyrin double-deckers.[1−21] All that activity prompted us to synthesize gadolinium and samarium bisporphyrinate complexes with various ligands: $Ln^{III}(oep)_2$, $Ln^{III}H(oep)(tpp)$, and $Ln^{III}H(tpp)_2$

* Author to whom correspondence should be addressed. Phone: ++30.81.393636. Telefax: ++30.81.393601 or 393671. E-mail address: coutsole@chemistry.uoc.gr.

[†] Université Paris XI.

[‡] University of Crete.

[§] University of Latvia-Kengaraga 8.

[||] Université Paris V.

(1) Buchler, J. W.; De Cian, A.; Fischer, J.; Kihn-Botulinski, M.; Weiss, R. *Inorg. Chem.* **1988**, *27*, 339.
(2) Buchler, J. W.; Scharbert, B. *J. Am. Chem. Soc.* **1988**, *110*, 4272.
(3) Buchler, J. W.; Kapellmann, H. G.; Knoff, M.; Lay, K. L.; Pfeifer, S. *Z. Naturforsch.* **1983**, *38b*, 1339.
(4) Duchowski, J. K.; Bocian, D. F. *J. Am. Chem. Soc.* **1990**, *112*, 3313.
(5) (a) Deisenhofer, J.; Epp, O.; Miki, K.; Huber, R.; Michel, H. *Nature (London)* **1985**, *318*, 618. (b) Deisenhofer J.; Epp, O.; Miki, K.; Huber, R.; Michel, H. *J. Mol. Biol.* **1984**, *180*, 385.
(6) Buchler, J. W.; Elsässer, K.; Kihn-Botulinski, M.; Scharbert, B. *Angew. Chem., Int. Ed. Engl.* **1986**, *25*, 286.
(7) Buchler, J. W.; Kihn-Botulinski, M.; Löffler, J.; Scharbert, B. *New J. Chem.* **1992**, *16*, 545.
(8) Buchler, J. W.; De Cian, A.; Fischer, J.; Hammerschmitt, P.; Weiss, R. *Chem. Ber.* **1991**, *124*, 1051.
(9) Buchler, J. W.; De Cian, A.; Fischer, J.; Kihn-Botulinski, M.; Paulus, H.; Weiss, R. *J. Am. Chem. Soc.* **1986**, *108*, 3652.
(10) Buchler, J. W.; De Cian, A.; Fischer, J.; Hammerschmitt, P. Löffler, J.; Scharbert, B.; Weiss, R. *Chem. Ber.* **1989**, *122*, 2219.
(11) Kim, K.; Lee, W. S.; Kim, H. J.; Girolami, G. S.; Gorlin, P. A.; Suslick, K. S. *Inorg. Chem.* **1991**, *30*, 2652.
(12) Donohoe, M.; Duchowski, J. K.; Bocian, D. F. *J. Am. Chem. Soc.* **1988**, *110*, 6119.
(13) Pitié, M.; Casas, C.; Lacey, C. J.; Pratviel, G.; Bernadou, J.; Meunier, B. *Angew. Chem.* **1993**, *32*, 557.
(14) Perng, J. H.; Duchowski, J. K.; Bocian, D. F. *J. Phys. Chem.* **1990**, *94*, 6684.
(15) Spyroulias, G. A.; Raptopoulou, C. P.; de Montauzon, D.; Mari, A.; Poilblanc, R.; Terzis, A.; Coutsolelos, A. G. *Inorg. Chem.* **1999**, *38*, 1683.
(16) Spyroulias, G. A.; Raptopoulou, C. P.; Terzis,; Coutsolelos, A. G. A. *Inorg. Chem.* **1995**, *34*, 2476.
(17) Spyroulias, G. A.; Coutsolelos, A. G. *Inorg. Chem.* **1996**, *35*, 1382.
(18) Ng, D. K. P.; Jiang, J. *Chem. Soc. Rev.* **1997**, *26*, 433.

10.1021/ic000410o CCC: $20.00
Published on Web 10/25/2001

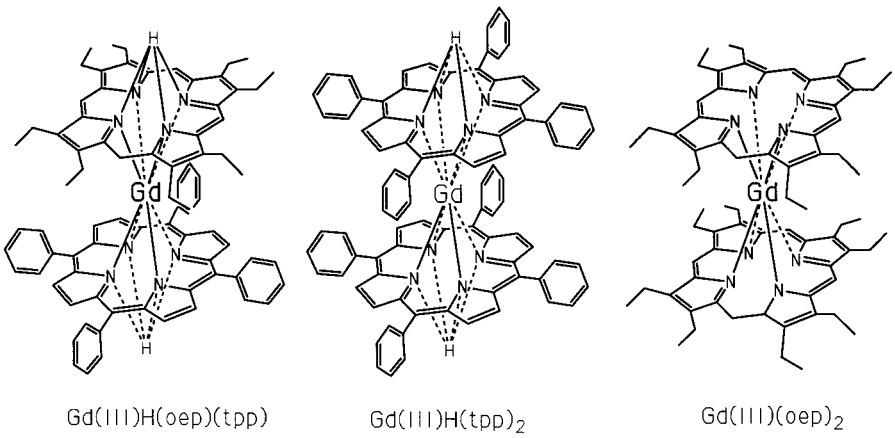

Figure 1. The three combinations for gadolinium bisporphyrinate complex schemes.

(where oep = octaethylporphyrin and tpp = tetraphenylporphyrin, see also Figure 1), in an effort to be able to target derivatives which may be used as artificial batteries.

Buchler et al. have reported the structure and electronic properties of sandwich-like lanthanoid (Ln^{IV} and Ln^{III}) bisporphyrinates.[2,6−9] The formula $Ln^{IV}(oep)_2$ (starting with Ce^{IV} as well as Zr^{IV}, Hf^{IV}, Th^{IV}, etc.) can be explained in terms of porphyrin ligands being present in the complexes as dianion $(oep)^{2-}$, while the formula $Ln^{III}(oep)_2$ can only be explained in terms of one porphyrin ligand being present in the complexes as dianion $(oep)^{2-}$ and the other as radical monoanion $(oep)^{-\cdot}$. Sandwich-like lanthanoid bisporphyrinates have been thoroughly investigated, and their physicochemical characterization by UV, ESR, and Raman spectroscopies has been reported,[1−3,6−20] but there are very few studies by EXAFS spectroscopy. Also spectroscopic studies like UV−visible, ^{1}H NMR, FT-IR, and EPR as well as electrochemical experiments have been improved on them, in order to enhance their redox behavior and particularly the influence of the strong $\pi-\pi$ interactions between the two macrocycles.[1−3,6−20]

We previously have reported the synthesis, electrochemical, and spectroscopic properties for analogous complexes.[15−17] Unfortunately only on the asymmetrical $Gd^{III}H(oep)(tpp)$ and $Sm^{III}H(oep)(tpp)$ complexes were X-ray diffraction data obtained (see Figure 2). Single crystals suitable for X-ray diffraction analysis have not been obtained for the symmetrical gadolinium [$Gd^{III}(oep)_2$ and $Gd^{III}H(tpp)_2$] and samarium [$Sm^{III}(oep)_2$ and $Sm^{III}H(tpp)_2$] dimers, despite the existence in the literature of crystallographic data for symmetrical Ce^{4+}, Zr^{4+}, and Eu^{3+} complexes, especially with the (oep) ligand.[1,9,11] In fact, the crystallization of this kind of derivative is extremely difficult, and this is probably due to the incorporation of solvent molecules during the preparation−purification process and/or their two forms, the protonated form and the deprotonated form.

However, the questions concerning the determination of structural parameters for the noncrystallized derivative, as well as the influence of some factors such as temperature and the presence of protonated forms for our double-deckers, warrant further study.

Continuing the effort to investigate this family of derivatives, we report herein the comparative X-ray absorption spectroscopy study (EXAFS and XANES) of bisporphyrinate $Ln^{III}(oep)_2$, $Ln^{III}H(oep)(tpp)$, and $Ln^{III}H(tpp)_2$ complexes, where Ln = Gd or Sm. As we mentioned before, we have carried out EXAFS

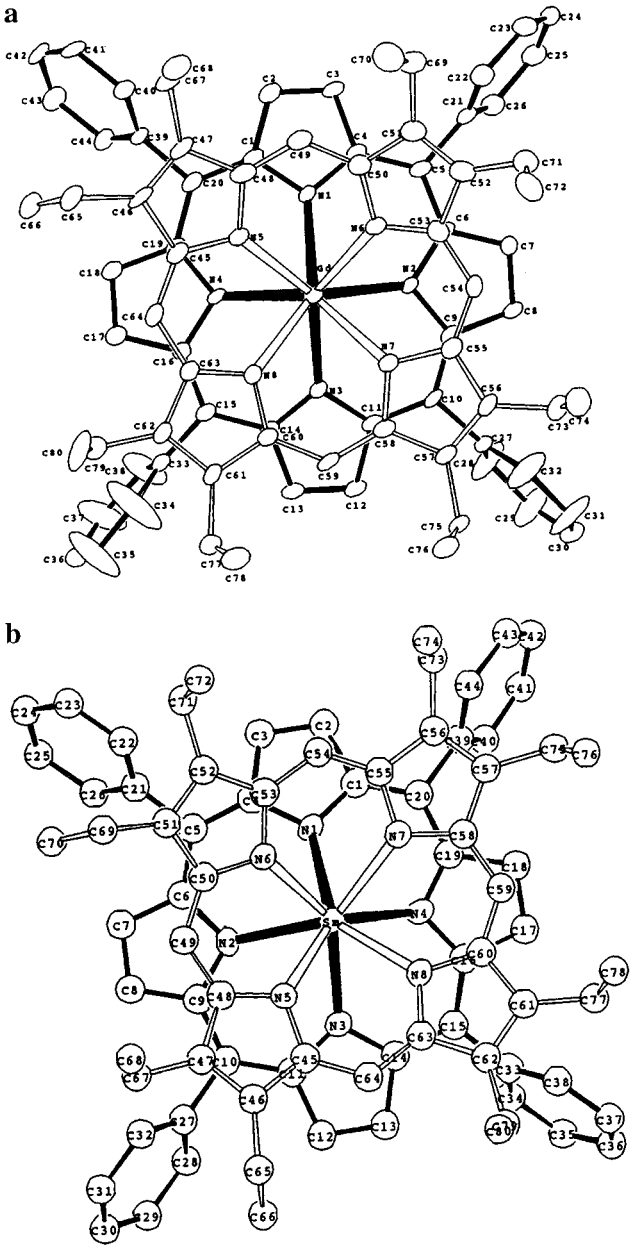

Figure 2. $Gd^{III}H(oep)(tpp)$ and $Sm^{III}H(oep)(tpp)$ complex structures (refs 15 and 16).

(19) Jiang, J.; Choi, M. T. M.; Law, W.-F.; Chen, J.; Ng, D. K. P. *Polyhedron* **1998**, *17*, 3903.
(20) Jiang, J.; Choi, M. T. M.; Law, W.-F.; Chen, J.; Ng, D. K. P. *Chem. Lett.* **1999**, 261.
(21) Girolami, G. S.; Milam, S. N.; Suslick, K. S. *J. Am. Chem. Soc.* **1988**, *110*, 2011.

analysis procedures with experimental phases and amplitudes as well as ab initio multiple scattering (MS) calculations; thus, we were able to obtain additional information about the structure of the first coordination shell of the protonated and nonprotonated complexes. We also attempted to analyze higher shells by including multiple scattering effects on the XAFS signals up to 5 Å, and the global results are discussed below.

Experimental Section

General Information. Dichloromethane (CH_2Cl_2) and 1,2,4-trichlorobenzene (1,2,4-tcb) were purchased from Riedel-de Häen and Aldrich, respectively, and used as received. Tetrahydrofuran (THF) was purchased from Merck and distilled under an argon atmosphere over a mixture of sodium−benzophenone. All syntheses were performed under an argon stream atmosphere using Schlenk-tube techniques. Pentanedione [acac(H)] and all lanthanide salts in the form of chlorides or nitrates were purchased from Aldrich and used as received. The (tpp)H_2 free base was synthesized according to a reported method,[22] (oep)H_2 was synthesized by a modified process,[23] and the metalation reactions were performed by the acetylacetonate method.[24]

Synthesis of Neutral Complexes $Ln^{III}H(oep)(tpp)$ and $Ln^{III}H(tpp)_2$. Lanthanide(III) monoporphyrinates, Ln^{III}(tpp)acac, with Ln = Gd, Sm, were prepared according to well-established experimental procedures.[24] The synthesis of the corresponding homo- and heteroleptic double-deckers $Ln^{III}H(tpp)_2$ and $Ln^{III}H(oep)(tpp)$ was carried out as follows: The freshly prepared Ln^{III}(tpp)acac (0.500 g, 0.570 mmol) was refluxed in 1,2,4-tcb for 3−5 h with 0.350 g (0.654 mmol) of Li_2(oep), prepared in situ according to the method published for $Sm^{III}H$-(oep)(tpp).[16] The reaction mixture was then allowed to cool to room temperature (RT). The isolation of all the complexes was achieved in four column chromatography steps.[15]

XAFS Measurements. The Gd L_3 edge spectra were recorded on the XAS2 beamline in transmission mode at the LURE-DCI storage ring (ring current, 350−250 mA; beam energy, 1.85 GeV) at low (80 K) and room temperature. The Sm L_3 edge spectra were collected on the XAS13 beamline and only at room temperature. We used a Si-(311) double-crystal monochromator, and 50% of harmonic rejection was achieved by slightly detuning the two crystals from the parallel alignment. The experimental spectra were measured by two ionization chambers filled with air with a step of 1 eV, and a count rate of 2 s per point, the energy resolution (fwhm) being 2.0 eV. The white line edge positions were reproducible with a precision of 0.2 eV (see XANES in Figure 3). A white line characteristic of a 2p−5d transition has been observed.

The microcrystalline powder samples were finely ground and pressed into a pellet supported with Kapton tape windows. The variations of the XAFS spectra related to the slit width were studied and adjusted in order to obtain spectra well defined for the data analysis.[25] The adjusted thickness of the sample permitted us to reach a value for the absorption jump between 0.5 and 1. So, a total of 4 scan data were recorded for each sample (about 2 h per spectrum), and each spectrum was individually checked before averaging.

XAFS Data Analysis. The following procedure was performed for our XAFS data analysis. First, the parameters for the $Ln^{III}H(oep)(tpp)$ complex were found, and then the structural parameters for the symmetrical complexes $Ln^{III}(oep)_2$ and $Ln^{III}H(tpp)_2$ were refined. As it is well-known,[26] in order to obtain structural parameters concerning the coordination sphere around a metal ion by using XAS techniques, it is necessary to know the backscattering phases and amplitudes. These two parameters could be obtained by two different approaches: the first one is measured from the experimental data on a related crystalline form, and the second one is from theoretical calculations that give directly these electronic functions, but here, there is a lack of knowledge of damping amplitude factors.

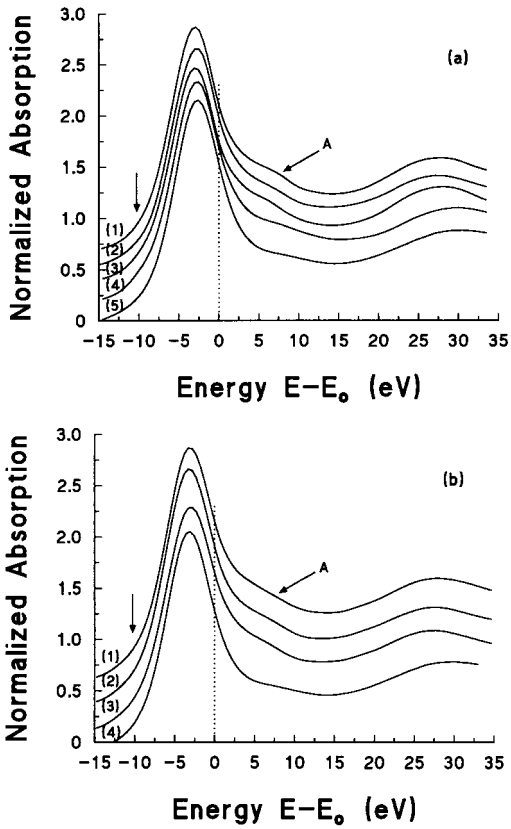

Figure 3. XANES spectra of the gadolinium (a) and samarium (b) complexes: $Ln^{III}(oep)_2$ complex (1), $Ln^{III}H(oep)(tpp)$ complex (2), and $Ln^{III}H(tpp)_2$ complex (3). The reference spectra (4) of well-known Gd^{3+} and Sm^{3+} aqua ions (0.2 M aqueous solutions) are shown. Finally, the spectrum of monoporphyrinate Gd^{III}(tpp)acac complex (5) is also given. All spectra are plotted on the same vertical scale and displaced vertically for clarity. All spectra are shifted to the corresponding E_0 positions.

Quantitative analyses were performed with experimental and theoretical standards.[26] The experimental data were analyzed with the EXAFS data analysis software package "EDA",[27] which has already been used in other cases.[28,29] For the derivatives with known X-ray analysis data, we had to constrain the parameters in order to get integer values of occupation number, with the same DW factor for similar types of atoms, at similar distances from Ln.[30,31] Particular attention was devoted to the XAFS zero-line removal (background and multielectron contributions) through the multistep polynomial/cubic-spline procedure.[32] The obtained XAFS signals, $\chi(E)$, were converted to the k space of the photoelectron wavevector, defined as $k = [(2m/\eta^2)(E - E_0)]^{1/2}$, where $(E - E_0)$ is the photoelectron kinetic energy measured. In the case of the L_3 edge of rare-earth elements, E_0 is located at 3.2 eV above the white line maxima. The experimental XAFS signal $\chi(k)$ was multiplied by a factor k^2 to compensate the decrease in its amplitude with the increase in the wavevector value (see Figure 4).

Figure 5 shows the Fourier transforms (FTs) of the experimental XAFS signals, with a Kaiser−Bessel window in the range 0.0−13.0 Å^{-1}. Modulus and imaginary parts of the FTs are not corrected for the

(22) Adler, A. D.; Longo, F. R.; Kampus, F.; Kim, J. *J. Inorg. Nucl. Chem.* **1967**, *32*, 476.
(23) Whittlock H. W.; Hanauer, R. *J. Org. Chem.* **1968**, *33*, 2169−2175.
(24) Wong, C. P.; Veinteicher, R. F.; Horrocks, W. D., Jr. *J. Am. Chem. Soc.* **1974**, *96*, 4149−4151.
(25) Maclean, A. L.; Foran, G. J.; Kennedy, B. J.; Turner, P.; Hambley, T. W. *Aust. J. Chem.* **1996**, *49*, 1273.
(26) Stern, E. A.; Sayers, D. E.; Lytle, F. W. *Phys. Rev.* **1975**, *B11*, 4836.
(27) Kuzmin, A. *Physica B* **1995**, *208*, 40.
(28) Bénazeth, S.; Purans, J.; Chalbot, M.-C.; Nguyen-van-Duong, M. K.; Nicolas, L.; Keller, F.; Gaudemer, A. *Inorg. Chem.* **1998**, *37*, 3667.
(29) Rocca, F.; Kuzmin, A.; Purans, J.; Mariotto, G. *Phys. Rev.* **1994**, *B50*, 6662.
(30) Co, M. C.; Hodgson K. O. *J. Am. Chem. Soc.* **1981**, *103*, 3200.
(31) Binsted, N.; Strange R. W.; Hasnain S. S. *Biochemistry* **1992**, *31*, 12117.
(32) Kuzmin, A.; Purans, J.; Benfatto, M.; Natoli, C. R. *Phys. Rev.* **1993**, *B47*, 2480.

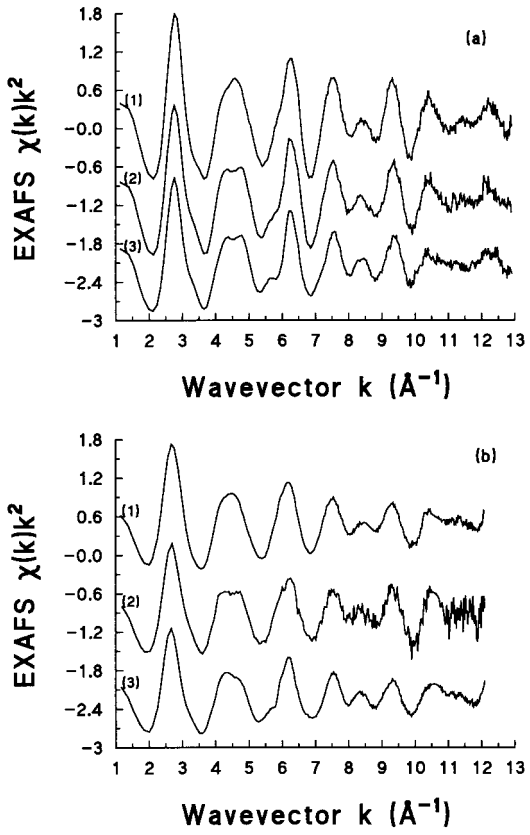

Figure 4. Experimental XAFS spectra $\chi(\kappa)\kappa^2$ of the gadolinium (a) and samarium (b) complexes: $Ln^{III}(oep)_2$ complex (1), $Ln^{III}H(oep)(tpp)$ complex (2), and $Ln^{III}H(tpp)_2$ complex (3). All spectra are plotted on the same vertical scale and displaced vertically for clarity.

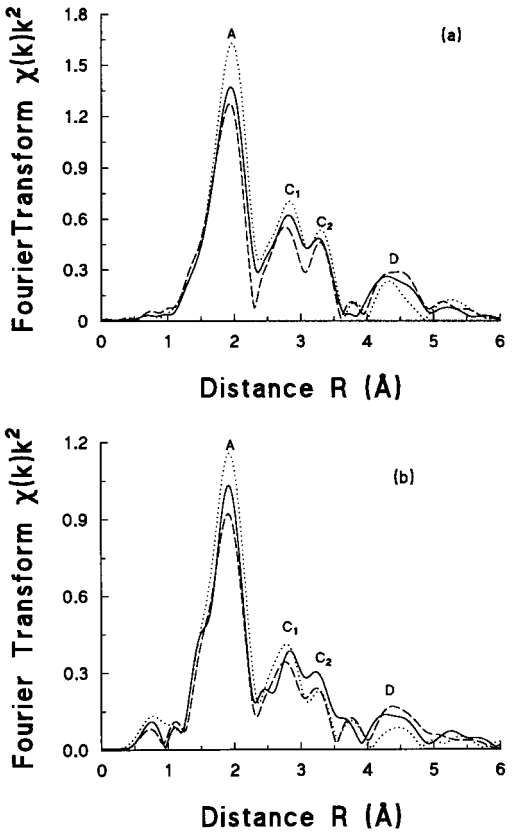

Figure 5. FTs (modulus part) of the experimental XAFS spectra of the gadolinium (a) and samarium (b) complexes: $Ln^{III}(oep)_2$ complex (dotted line), $Ln^{III}H(oep)(tpp)$ complex (solid line), $Ln^{III}H(tpp)_2$ complex (dashed line).

photoelectron phase shift; therefore the positions of peaks differ from the true crystallographic values at about 0.5 Å. As one can see (Figure 5), four main peaks are present in the experimental FTs: first main peak located at 1.2−2.2 Å with a maximum at 1.94 Å (label A) representing the Ln−N first shell; two peaks located at 2.5−3.2 Å with maximums at 2.8 and 3.25 Å, respectively (labeled C_1 and C_2); and a smaller peak (labeled D) at longer distances around 3.9−4.9 Å with a maximum at 4.25 Å.

We will proceed by presenting step by step our analysis for text clarity. So, in this context we will start with the first shell XAFS signal analysis. The first shell XAFS signals were singled out by the back FT procedure in the range between 0.6 and 2.4 Å. Calculations of the XAFS function were based on the single scattering curved-wave formalism. The first shell XAFS signals were fitted using an anharmonic one-shell model by a cumulant expansion:[33,34]

$$\chi(k) = \frac{N}{kR^2} f(\pi,k) \exp\left(-2C_2k^2 + \frac{2}{3}C_4k^4\right) \sin\left(2kR - \frac{4}{3}C_3k^3 + \phi(\pi,k)\right)$$

where N is the coordination number, R is the interatomic distance, and σ_i is the Debye−Waller (DW) factor (in harmonic approximation $C_2 = \sigma_i^2$). The DW of the lanthanide complexes can be described as the sum of σ^2_{stat}, due to static disorder and σ^2_{vib}, due to thermal vibrations.[35] The higher-order cumulants C_3 and C_4 characterize the deviation of the distribution of distances from a Gaussian shape. In a second step, we proceed to the decomposition of the first shell in a two-shell model. For this, we fitted using standard harmonics (C_3 and $C_4 = 0$), in which the radial distribution function (RDF) is taken into account by a superposition of two Gaussian distributions.

The backscattering amplitude and phase functions were obtained using two approaches: the experimental and the theoretical one. The experimental backscattering amplitude $f(\pi,k)$ and phase $\phi(\pi,k)$ functions were extracted from the XAFS data of the $Ln^{III}(oep)_2$ derivatives: Gd−N (R = 2.50 Å, DW = 0.004 Å^2); Sm−N (R = 2.53 Å, DW = 0.006 Å^2). We expected for $Ln^{III}(oep)_2$ complexes an increase of Ln−N distance in the series $Gd^{3+} < Eu^{3+} < Sm^{3+}$ according to the increase in the ionic radii: 1.06 < 1.07 < 1.09 Å. The calculated distances are in agreement with previously published XRD data by Buchler et al. for the $Eu(oep)_2$ complex (Eu−N = 2.510 Å).[1]

The theoretical backscattering functions were calculated for the clusters as following: distorted antiprism LnN_8 (first shell of the dimeric complexes) with the distance Ln−N (R = 2.50 Å), and the typical values of the muffin tin radii: $R_{mt}(Ln) = 1.56$, $R_{mt}(N) = 0.71$ Å. We must affirm here that the distorted antiprism LnN_8 mimics the structure of the title complexes. Since the initial energy E_0 of the photoelectron is defined in the FEFF6 code[36] relative to the Fermi level E_F and strongly depends upon the muffin tin radii, we chose the continuum threshold (3.2 eV above the white line maximum). The photoelectron mean free path contribution was automatically included in the scattering amplitude function using the complex Hedin−Lundqvist (HL) exchange and the correlation potential (ECP). A natural broadening was included through the core level width $\Gamma_{core-hole}$ = 3.5 eV for the $2p_{3/2}$ level in the case of the Gd and Sm L_3 edges.

MS XAFS Analysis. Considering the signatures observed beyond the first shell, we took care of the MS effects which are known to modify the amplitudes and phases of the XAFS signals. The MS calculations were performed using the FEFF6 code[36] on the clusters with different dimensions, constructed from the crystallographic data of $Ln^{III}H(oep)(tpp)$ derivatives.

The central Ln atoms of the clusters are stuck between two porphyrin macrocycles (see Figure 2, $Gd^{III}H(oep)(tpp)$ complex) and bound to

(33) Buncker, G. *Nucl. Instrum. Methods Phys. Res.* **1983**, *207*, 437.
(34) Dalba, G.; Fornasini, P.; Grisenti, R.; Purans, J. *Phys. Rev. Lett.* **1999**, *82*, 4240.
(35) Yamaguchi, T.; Nomura, M.; Wakita, H.; Ohtaki, H. *J. Chem. Phys.* **1988**, *89*, 5153.
(36) Rehr, J. J.; Mustre de Leon, J.; Zabinsky, S. I.; Albers, R. C. *J. Am. Chem. Soc.* **1991**, *113*, 5135−5140.

the eight nitrogen atoms with distances around 2.46−2.66 Å. The Ln position possesses C_1 symmetry, and the eight nitrogen atoms form a distorted square antiprism. The 16 pyrrolic carbon atoms, named C_α (3.42−3.61 Å), and the eight carbon atoms in meso positions, named C_μ (3.75−3.93 Å), create the second and third coordination shells, respectively. The last 16 carbon atoms of the pyrroles, named C_β (4.65−4.79 Å), form the fourth shell of Gd. The ligands ethyl and phenyl are further out from the central atom at 5.5 Å and are not included in the clusters; the distance is too long to be unambiguously extracted by XAFS analysis.

Therefore we carried out MS calculations for the clusters of 32 atoms within the 4.5 Å radius and with the cluster of 48 atoms within the 5.0 Å radius, taking into account all SS and MS paths up to the third order and with the muffin tin radii: $R_{mt}(Gd) = 1.56$ Å, $R_{mt}(N) = 0.70$ Å, $R_{mt}(C_\alpha) = 0.69$ Å, $R_{mt}(C_\mu) = 0.70$ Å, $R_{mt}(C_\beta) = 0.71$ Å.

Sharp double-electron excitations have been observed in the studied XAFS spectra. They are illustrated by the peaks with a width of several electronvolts located in the XAFS spectra about 6 $Å^{-1}$ (see Figure 4). In the case of the rare-earth L_3 edges, such signals have already been reported.[37−39] As it was mentioned earlier, the presence of the double-excitation contribution modifies the fine structure beyond the absorption edge. This automatically leads to the distortion of the XAFS signal (and consequently its FT) and, accordingly, increases the error in the determination of structural parameters. However, our analyses confirm that the influence of such effects on the FT was analogous to the effect of the steplike function, i.e., it produces a significant contribution only in the FT range above 5 Å.

Results

XANES Data. Figure 3 represents the XANES spectra (shifted to the corresponding E_0 positions) of the studied gadolinium and samarium complexes. All spectra are normalized and displaced vertically for clarity. For the comparison, the well-known reference spectra of Gd^{3+} and Sm^{3+} aqua ions (0.2 M aqueous solutions) are shown. Finally, the spectrum of monoporphyrinate Gd^{III}(tpp)acac complex is also included. As one can easily distinguish within the two series (Gd and Sm), the white line (WL) maximum positions coincide with each other (experimental precision 0.2 eV).

The presence of two valence states (Ln^{2+} and Ln^{3+}) can easily be distinguished by XANES spectroscopy due to their different position of WL (about 8 eV) which corresponds to the transition to unoccupied 5d states.[40] In our case, no traces of Ln^{2+} ions were detected: the arrow indicates the expected WL position of Ln^{2+} ions. Therefore, the obtained experimental XANES spectra (Figure 3) are in good agreement with the expected spectra concerning the +3 oxidation state.

All XANES spectra of the studied bisporphyrinates present a great similarity, which confirms the similarity of the structures of these complexes. A characteristic shoulder (A) is observed which has been attributed to the MS contribution. Previously, Natoli and co-workers[41] published the MS calculation on a square antiprism configuration of Ln complexes[42,43] and have stressed that the shoulder (A) is a characteristic MS contribution, resulting from the constructive interferences between the two planes, and provides insights for the relative orientation between the lower and upper planes. Moreover, the previous XRD investigations on the Ln bisporphyrinates show that the coordination polyhedron of Ln^{3+} is a square antiprism where the two porphyrin rings are rotated about 45°.[9,16] On the ORTEP diagram[16] of the GdH(oep)(tpp) (Figure 2), the coordination polyhedron of the Gd(III) is shown, which is a square antiprism with the two porphyrin rings, rotated by an angle of 45°.

However, an interesting question was how the symmetrical compounds are packed. A reasonable answer for that can be given after the analysis of XANES curves. As we have stressed before, all the XANES spectra of the bisporphyrinates present a very similar form. Therefore we can use the spectra of known complexes as a fingerprint for the identification of unknown structure. Note that feature A is very well defined in all spectra for our Gd and Sm bisporphyrinate derivatives. On the other hand, the XANES spectra of the Gd^{3+} and Sm^{3+} aqua ions (tricapped prism) and monoporphyrinate Gd^{III}(tpp)acac complex present a significantly smaller amplitude for the shoulder (A) in question. Therefore we suggest that antiprism coordination is more favorable for the Gd and Sm bisporphyrinates studied.

Experimental XAFS spectra for the Ln L_3 edge of the $Ln^{III}(oep)_2$, $Ln^{III}H(oep)(tpp)$, and $Ln^{III}H(tpp)_2$ complexes in the crystalline state at low and room temperatures (for Gd and Sm) are presented in Figure 4. The XAFS spectra are very similar between the corresponding Gd and Sm complexes, and that confirms the similarity between those two series of complexes. Also, the XAFS spectra of Gd at low and room temperatures exhibit a normal temperature dependence (increase of the Debye−Waller factor with temperature); that confirms the reproducibleness of the XAFS measurements.

Furthermore, the features of the XAFS signals are very similar in the protonated forms $Ln^{III}H(oep)(tpp)$ and $Ln^{III}H(tpp)_2$ and different from those in $Ln^{III}(oep)_2$ complexes. Under the same conditions and inside the recorded sets of measurements, the same ratio between the oscillation amplitudes of the XAFS spectra (8:7:6 for the $Ln^{III}(oep)_2$, $Ln^{III}H(oep)(tpp)$, and $Ln^{III}H(tpp)_2$, respectively) has been observed.

The experimental XAFS spectra were Fourier transformed, and their FTs are presented in Figure 5. The first peak on the FTs corroborates the feeling about the XAFS amplitude: the $Ln^{III}H(tpp)_2$ has an abnormal lower amplitude of its first peak in comparison to that of the $Ln^{III}(oep)_2$. Those differences are related to protonated and nonprotonated forms for the studied complexes as we will discuss below.

A recurrent phenomenon either with Gd or with Sm is the decreasing amplitude of the first peak from $Ln^{III}(oep)_2$ to $Ln^{III}H(oep)(tpp)$ and $Ln^{III}H(tpp)_2$ complexes. This fact has prompted us to investigate the influence of protonation or not of our complexes and its influence on the Ln−N distance. It appears that the proton has the tendency to displace the macrocycle on which it resides, providing one large distance Ln−N−(H) in the protonated species. The XRD provides for the $Ln^{III}H(oep)(tpp)$ derivatives, distances Gd−N(7) = 2.65 and Sm−N(7) = 2.62 Å, much larger than the other Ln−N distances.

It was hitherto reported that the proton prefers residing on the more basic OEP nitrogen atom than that on TPP with a ratio $N-H_{tpp}/N-H_{oep}$ equal to 1:4.3 based on ^1H NMR data.[17] That implies a $Ln-N_{oep}$ distance superior to the other $Ln-N_{oep}$ or $Ln-N_{tpp}$ distances. We assume that the protonated bond Ln−N−(H) gives a weak contribution to XAFS spectra and creates an asymmetry in the radial distribution function. The above assumption also could explain the highest amplitude observed for the nonprotonated $Ln^{III}(oep)_2$ complex.

(37) Solera, J. A.; Garc£a, J.; Proietti, M. G. *Phys. Rev.* **1995**, *B51*, 2678.
(38) Purans, J.; Kuzmin, A.; Burattini, E. *Jpn. J. Appl. Phys.* **1993**, *32*, Suppl. 32-2, 64.
(39) Benazeth, S.; Tuilier, M. H.; Guittard, M. *Physica B* **1989**, *158*, 39.
(40) Ravot, D.; Godard, C.; Achard, J. C.; Lagarde, P. In *Valence Fluctuations in Solids*; Falicov, H. M., Ed.; North-Holland Publishing Company: Amsterdam, 1981; p 423. Antonio, M. R.; Soderholm, L. *J. Appl. Electrochem.* **1997**, *27*, 784.
(41) Wu, Z.; Benfatto, M.; Natoli, C. R. *Phys. Rev. B* **1998**, *57*, 10336.
(42) Tan, Z. Q.; Budnick, J. I.; Chen, W. Q.; Brewe, D. L. *Phys. Rev. B* **1990**, *42*, 4808.
(43) Koike, N.; Uekusa, H.; Ohashi, Y.; Harnoode, C. *Inorg. Chem.* **1996**, *35*, 5798.

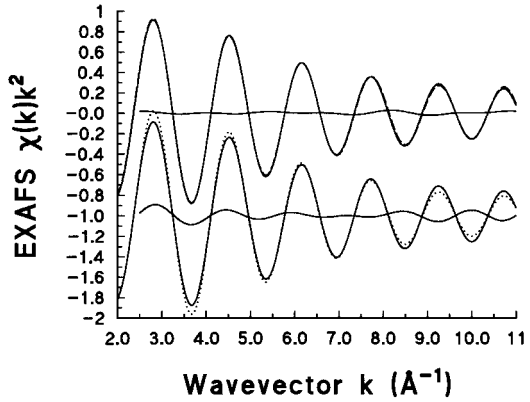

Figure 6. Best fit of first shell using experimental phases and amplitudes: the experimental XAFS for the GdH(oep)(tpp) complex at LT (solid line); two shell model fit with constraints $N_1 = 7$, $N_2 = 1$, and $C_3 = 0$ and residual (dashed line); one shell model fit with constraints $N = 8$, $C_3 = 0$ and residual (dotted line).

In the case now of the protonated compounds, two different factors could play an important role on the inter-ring distance: the presence of the proton moving the (oep) macrocycle away from the central Ln^{3+} atom more than the (tpp) macrocycle, and the steric effect[44] due to the phenyl substituents reducing the distance between the two porphyrinic rings and making the (tpp) cycle closer to the photoabsorber.

First Coordination Shell Fitting Results. The SS contributions, related to the first shell, were singled out by the back FT in the intervals 0.6−2.4 Å ($\Delta R = 1.8$ Å). The best fit of the XAFS signal analysis was performed in the k range from 2.0 to 11.0 Å^{-1} ($\Delta k = 9.0$ Å^{-1}). The maximum number of fitting parameters N_{ind} is about 12 ($\Delta k = 9.0$ Å^{-1} and $\Delta R = 1.8$ Å), and N_{ind} is limited by the number of independent data points $N_{ind} \cong 2\Delta k \Delta R/(\pi + 2)$.[45] The number of fitting parameters is significantly smaller. For the Gd and Sm bisporphyrinate complexes, one-shell ($Ln-N_{av}$) and two-shell ($Ln-N_1$, $Ln-N_2$) contribution models are used. The analysis with constant coordination number was performed for the two-shell model. We took four fitting parameters as for one contribution (N, R, DW, C_3), and as for two contributions (R_1, DW_1, R_2, DW_2). The above analysis with the two-shell model is in agreement with the analysis for the Gd and Sm complexes, and that for the eight nitrogen atoms of the bisporphyrins. In contrast, the one-shell model gave unreasonable coordination numbers for the protonated complexes, or great fitting error with reasonable coordination number (see for example Figure 6).

A summary of the best-fit analysis between the theoretical (feff) and experimental (ref) phases and amplitudes for the first coordination shell is presented in Table 1. For convenience, the best fits obtained using one- and two-shell models for the $Gd^{III}H(oep)(tpp)$ complex are shown in Figure 6. The results of this analysis including asymmetry of the RDF (C_3 cumulant) with the theoretical phases and amplitudes are presented in the Table S.1 as Supporting Information. Note that, in Table 1, only the fitting procedures labeled (feff) give the absolute values of the structural parameters, while the fitting procedures label (ref) give the small fitting error and high accuracy of relative changes between the different samples.

On the basis of the fitting parameters, the radial distribution function (RDF) can be reconstructed according to the equation of the sum of Gaussian distributions.[27,29] As we mentioned before, this graphical representation (see Figure 7) is very useful since it takes into account not only the coordination numbers and the peak positions but also the DW factor values (static and dynamic part), and overlaps from the different shell contributions.

Table 1. First Coordination Shell Structural Data Obtained from the Best-Fit Analysis of the Ln Complexes with the One- and Two-Shell Fitting Models[a]

	bonds Gd−N				bonds Sm−N			
state	N_1	R_1 (Å)	σ_1^2 (Å^2)	$\epsilon \times 10^{-3}$	N_1	R_1 (Å)	σ_1^2 (Å^2)	$\epsilon \times 10^{-3}$
				$Ln^{III}(oep)_2$				
LT(feff)	8.0	2.50	0.004	3.4				
LT(ref)[b]	8.0	2.50	0.004					
RT(feff)	8.1	2.50	0.006	3.4	8.0	2.53	0.006	3.2
RT(ref)[b]	8.0	2.50	0.006	0.1	8.0	2.53	0.006	
				$Ln^{III}H(oep)(tpp)$				
LT(feff)	7.2	2.49	0.005	3.0				
LT(ref)	7.0	2.49	0.005	0.1				
LT(ref)	7.0[c]	2.48	0.005	0.1				
	1.0[c]	2.65	0.007					
RT(feff)	7.1	2.49	0.006	2.4	6.7	2.53	0.006	1.7
RT(ref)	6.9	2.46	0.006	0.3	6.5	2.52	0.005	0.1
RT(ref)	7.0[c]	2.46,	0.006,	0.4	7.0[c]	2.51,	0.005,	0.1
	1.0[c]	2.65	0.008		1.0[c]	2.73	0.006	
				$Ln^{III}H(tpp)_2$				
LT(feff)	6.3	2.50	0.006	2.2				
LT(ref)	6.1	2.50	0.006	0.3				
LT(ref)	6.0[c]	2.45	0.007	0.2				
	2.0[c]	2.65	0.007					
RT(feff)	6.4	2.50	0.008	2.2	6.4	2.50	0.006	1.5
RT(ref)	6.1	2.50	0.008	0.4	6.3	2.50	0.006	0.3
RT(ref)	6.0[c]	2.45,	0.007,	0.2	6.0[c]	2.49,	0.006,	0.2
	2.0[c]	2.66	0.009		2.0[c]	2.73	0.007	

[a] The label (feff) indicates theoretical while (ref) indicates experimental phases and amplitudes. N is the number of atoms located at the distance R from the Ln, σ^2 is the DW factor, and ϵ is the fitting error.[27] The one-shell (feff) absolute errors are ±0.5 on N, ±0.02 Å on R, and ±0.001 Å^2 on σ^2. The relative error bars (ref) are lowered when we compare different measurements to ±0.3 on N, ±0.005 Å on R, and ±0.001 Å^2 on σ^2. The error bars for the two-shell fitting procedure are ±0.02 Å on R and ±0.001 Å^2 on σ^2 for the short distances and ±0.05 Å on R and ±0.003 Å^2 on σ^2 for the long distances. [b] The reference compound.The mean bond lengths Ln−N are calculated from the crystallographic data on the $Eu^{III}(oep)_2$ complex from ref 1. The DW factor is taken from the feff fitting procedure. [c] The coordination numbers are fixed.

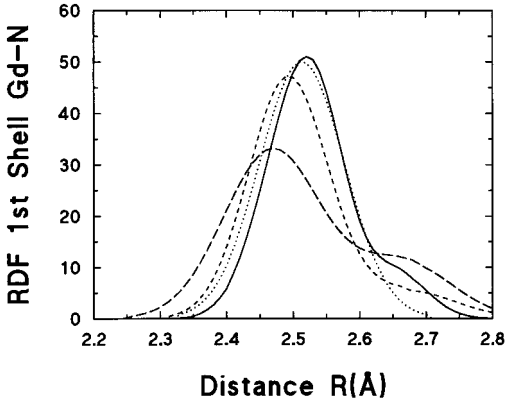

Figure 7. Reconstructed RDFs of the first coordination shell of the Gd complexes at LT. RDFs obtained from XAFS data [$Ln^{III}(oep)_2$ complex (dotted line), $Ln^{III}H(oep)(tpp)$ complex (dashed line), $Ln^{III}H(tpp)_2$ complex (long dashed line)] and based on the XRD data of $Ln^{III}H(oep)(tpp)$ (full line).

(44) Barkigia, K. M.; Renner, M. W.; Furenlid, L. R.; Medforth, C. J.; Smith, K. M.; Fajer, J. *J. Am. Chem. Soc.* **1993**, *115*, 3627.
(45) Report on the International Workshop on Standards and Criteria in XAFS. In *X-Ray Absorption Fine Structure*; Hasnain, S. S., Ed.; Ellis Horwood: New York, 1991; p 751.

MS XAFS Results. We present herein the MS calculations for a cluster of 32 atoms within a 4.5 Å radius around Ln and for a cluster of 48 atoms within a 5.0 Å radius, taking into account all SS and MS paths up to the third order. The comparison of MS and SS calculations for the clusters of different dimensions allowed us to assign different peaks on the experimental XAFS FT.

At this first step, we tried to understand qualitatively the nature of the peaks beyond the first coordination shell in the XAFS FTs and particularly about the MS contributions. As one can see in Figure 5, four main peaks are present in the experimental FTs: the first main peak located at 1.2−2.2 Å with a maximum at 1.94 Å (label A); two peaks located at 2.5−3.2 Å with maximums at 2.80 Å and at 3.25 (label C_1 and C_2, respectively); and the peak at 3.9−4.9 Å with a maximum at 4.25 Å (label D).

For the cluster of 32 atoms around the Gd, the SS and MS (total 112 paths) calculated spectra within the radius 4.5 Å are shown in Figure S1 in comparison with the experimental one. The SS calculation (32 paths) is surprisingly in good agreement with the experiment. The modulus and imaginary parts of these FTs coincide well too. The MS signals (80 paths) give only small distortion of the form of the SS contributions (Figure S1.a). The modulus (see Figure S2.a) and imaginary parts of these FTs coincide well too. The MS signals produce some contribution in the EXAFS region and to the FT peaks C_1 and C_2, but it seems that the MS signals produce small contribution in the experimental spectra. This result is mainly due to the interference effect between MS signals and, possibly, structural and/or thermal disorder. As one can see in Figure S1, the DS and TS signals present the opposite phase that leads to a decrease of the total MS signal amplitude. The most important MS signal generated within the Gd−N−C_α chains originates from the eight pyrrolic groups: 32 DS contributions with path lengths of 3.6−3.8 Å and amplitude ratio 6%.

For the cluster of 48 atoms around the Gd, the SS and MS (total 435 paths) calculated XAFS and FT spectra are shown in Figures S1.b and S2.b, respectively. The 16 peripheral carbon atoms C_β (4.65−4.79 Å) generate SS contributions (15% amplitude), but also strong DS and TS contributions within near linear Gd−N−C_β chains originate from the eight pyrrolic groups: 32 DS contributions with a path length about 4.8 Å and amplitude ratio 12% and 16 TS contributions with a path length about 4.8 Å and amplitude ratio 10%. The FT analysis shows that the D peak at 4.25 Å corresponds mainly to the MS contributions within Gd−N−C_β chains. Note that the number of carbon atoms (C_β) determined from the SS analysis of XAFS is three times less than the expected one. This result is mainly due to the interference effect between SS and MS signals. As a concequence, the fitting analysis of this region is complicated and beyond the scope of this paper.

To conclude MS analysis, we suggest that also on the experimental FTs the main first peak A corresponds to SS processes on the eight nitrogen atoms, the second and third ones (C_1 and C_2) correspond mainly to SS from the second and third shells around gadolinium ion formed by the 16 C_α and eight C_μ carbon atoms, and, finally, peak D corresponds to MS contributions within near linear Gd−N−C_β chains. Its amplitude is damped by the dispersion of the distances structural and thermal disorder.

Second and Third Coordination Shell Fitting Results. As previously mentioned, the C_1 and C_2 peaks of the FTs are attributed mainly to two SS contributions from the Gd surrounding second and third shells formed by 16 carbon (C_α) atoms at 3.23−3.52 Å and eight carbon (C_μ) atoms at 3.6−3.8 Å, respectively. However, we verified that the DS signal (Gd−N−C_α) can also produce some small contribution.

Table 2. Second Coordination Shell Structural Data Obtained from the Best-Fit Analysis of the Gd Complexes at LT and Sm Complexes at RT[a]

	bonds Ln−C_1			bonds Ln−C_2			
state	N_1	R_1 (Å)	σ_1^2 (Å^2)	N_2	R_2 (Å)	σ_2^2 (Å^2)	$\epsilon \times 10^{-3}$
			$Gd^{III}(oep)_2$				
XAFS	16[d]	3.46	0.004	8[d]	3.78	0.004	5.8
XRD[b]		3.47			3.80		
			$Gd^{III}H(oep)(tpp)$				
XAFS	16[d]	3.46	0.004	8[d]	3.78	0.004	6.1
XRD[c]		3.50			3.84		
			$Gd^{III}H(tpp)_2$				
XAFS	16[d]	3.46	0.007	8[d]	3.78	0.008	4.3
XRD							
			$Sm^{III}(oep)_2$				
XAFS	16[d]	3.45	0.009	8[d]	3.78	0.006	3.4
XRD[b]		3.47			3.80		
			$Sm^{III}H(oep)(tpp)$				
XAFS	16[d]	3.45	0.008	8[d]	3.77	0.006	3.4
XRD[c]		3.50			3.84		
			$Sm^{III}H(tpp)_2$				
XAFS	16[d]	3.45	0.010	8[d]	3.79	0.008	2.0
XRD							

[a] N is the number of atoms located in the ith shell at the distance R from the Gd, σ^2 is the DW factor, and ϵ is the fitting error. Absolute errors are ±0.03 Å on R and ±0.002 Å^2 on σ^2. This error bar is lowered when we compare different measurements to ±0.01 Å on R and ±0.001 Å^2 on σ^2. [b] The mean bond length Ln-C_{oep} is calculated from the crystallographic data on the $Eu^{III}(oep)_2$ complex from ref. Buchler [1]. [c] The data from ref. Spyroulias et al. [15, 16]. [d] The coordination numbers are fixed.

We included only more important MS contribution: the DS contribution within the Gd−N−C_α chain. The fitted parameters for each contribution were distances and DW factors that give 6 varying parameters. Nevertheless, the fitting results show that, due to a high DW factor, and to the behavior of the MS scattering amplitude, rapidly going down with the increase of the photoelectron energy, the MS contribution is present mainly at the beginning of the XAFS signal (up to 4 Å^{-1}). This allows to separate SS contributions from the MS one and to extract reliable information on the distances and DW factor of C_α and C_μ atoms, whose XAFS signal is well isolated at high wave vector values (4−13 Å^{-1}).

The contributions, related to the second and third shell, were singled out by the back FT in the intervals 2.3−3.7 Å (ΔR = 1.4 Å). The best fit analysis was performed in the k range from 4.0 to 12.0 Å^{-1} (Δk = 8.0 Å^{-1}) taking into account two SS contributions (Gd−C_α and Gd−C_μ) with 4 varying parameters. The fitted parameters for each contribution were distances and DW factors. The maximum number of fitting parameters N_{ind} is about 8 (Δk = 8 Å^{-1} and ΔR = 1.4 Å). Thus, if we also take two fitting parameters per contribution, the maximum number of contributions which can be used is four.

The summary of the best-fit analysis is presented in Table 2 and compared with the crystallographic data for $Ln^{III}(oep)_2$ and $Ln^{III}H(oep)(tpp)$. The XAFS values are in close agreement with the average mean bond lengths calculated from XRD data. The analysis shows that for gadolinium and respectively for samarium complexes the two-atom distribution (Gd−C_α and Gd−C_μ) remains the same with the average distances R(Gd−C_α) = 3.46 ± 0.03 Å and R(Gd−C_μ) = 3.78 ± 0.03 Å. The structural

disorder determined by XAFS $\sigma^2 = 0.004$ Å^2 for the distributions (Gd−C_α and Gd−C_μ) is slightly larger than the ones given by XRD. The obtained distances are in good agreement with known XRD data.

Discussion

$Ln^{III}(oep)_2$. Buchler et al.[1−3,6−10] have described the synthesis and physicochemical characterization of sandwich-like lanthanoid bisporphyrinates $Ln^{III}(oep)_2$ and have emphasized that the presence of two porphyrin ligands with the distinct negative charges −1 and −2 should cause different Ln−N bond lengths. However, the small differences (Eu−N: 2.514 and 2.506 Å) are not significant. Therefore, Buchler and co-workers have suggested either statistical disorder of two porphyrin ligands in different oxidation states or complete delocalization of the electron hole between the two cofacial π-electron systems of the porphyrin ligands.[1] As it was mentioned before, for $Ln^{III}(oep)_2$ complexes the increase in Ln−N distance in the series $Gd^{3+} < Eu^{3+} < Sm^{3+}$ must reflect an increase in the ionic radii: 1.06 < 1.07 < 1.09 Å, respectively.

The distances for the studied $Gd^{III}(oep)_2$ and $Sm^{III}(oep)_2$ complexes have been calculated from the X-ray structure of $Eu^{III}(oep)_2$. The results of fitting procedures (see Tables 1 and 2) are in good agreement with previously published XRD data.[1] The gadolinium ion is strongly bonded to the eight nitrogen atoms at R(Gd−N_{av}) 2.50 Å with a small DW factor. The DW factor increases with temperature from 0.004 to 0.006 Å^2 in agreement with the increase of the thermal motions. The samarium ion is also bonded to the eight nitrogen atoms at the distance R(Sm−N_{av}) 2.53 Å (in accordance with the ionic radii of Gd^{3+} and Sm^{3+}, the latter distance is larger) with the same DW factor 0.006 Å^2 at room temperature. Thus, we confirm the structural data obtained on $Eu^{III}(oep)_2$. Moreover, we exclude the proposed statistical disorder of two porphyrin ligands in different oxidation states stated by Buchler et al.[10] In fact, the sensitivity of the DW factor to the temperature, and its low value at 80 K measurements, is not consistent with an important part of the structural disorder related to various electronic charges on porphyrin ligands. So, the second assumption from Buchler on a complete delocalization of the hole between the two cofacial π-electron systems of the porphyrin ligands seems preferential.

$Ln^{III}H(oep)(tpp)$. The XRD data is only available for the asymmetrical $Gd^{III}H(oep)(tpp)$ and $Sm^{III}H(oep)(tpp)$ complexes.[15,16] At room temperature the mean bond length to the eight nitrogen atoms R(Gd−N_{av}) is 2.538 Å, while the distance to tpp porphyrin is a little shorter (2.524 Å) than for the oep porphyrin Gd−N(oep) (2.551 Å). At low temperature (21 K) as expected, the distances became smaller (2.516 and 2.548 Å, respectively) due to the thermal contraction. Concerning the longer Gd−N(oep) bond distance with respect to Gd−N(tpp), the authors have assumed the presence of the hydrogen in the oep ring. The one-shell model (feff and ref) gives an unreasonable coordination number (7) for gadolinium as well as for samarium. The gadolinium ion is strongly bonded to the seven nitrogen atoms at R(Gd−N_{av}) 2.49 Å with a small DW factor. The DW factor increases with temperature from 0.005 to 0.007 Å^2. The samarium ion is also bonded to the seven nitrogen atoms at expected larger distance R(Sm−N_{av}) 2.53 Å (according to the ionic radii of Gd^{3+} and Sm^{3+}) with the same DW factor 0.006 Å^2 at room temperature.

We introduce the two-shell model to mimic dispersion of the distances and especially to take into account the presence of one nitrogen atom at about 2.65 Å that creates strong asymmetry of RDF. The model matches the experimental signal as well as the one-shell model, and in addition has reasonable coordination number with respect to known XRD structure of the bisporphyrins. After this described analysis we conclude that the gadolinium and samarium ions are strongly bonded to the eight nitrogen atoms, but one nitrogen atom is located at significantly larger distance.

From first analysis and calculations on the XRD data of the bisporphyrinate, it seems that the RDF of Gd−N distances is represented by two Gaussians separated about 0.03 Å: the Gd−N(tpp) distance is 2.516 Å and that for Gd−N(oep) 2.548 Å. The inspection of the reconstructed RDF (broadened with DW factor 0.003 Å^2) shows only one peak at 2.52 Å with pronounced asymmetry (see Figure 7). The maximum of the RDF (approximately seven atoms) is shifted, approximately 0.05 Å compared to the average distance, and one atom gives the additional peak at about 2.64 Å. This is due to the fact that bond lengths Gd−N(oep) are very dispersed from 2.459 to 2.655 Å and the first seven distances have an average distance 2.516 Å. The XRD distance Gd−N for seven nitrogen atoms differs from the EXAFS distance at about 0.02 Å. The difference can be attributed to the asymmetry of the distribution of distances Gd−N, as a single scattering EXAFS analysis is very sensitive to the asymmetry of that radial distribution function (RDF) and generally gives shorter distances.

The XAFS RDFs reconstructed using experimental phases and amplitudes are presented on the Figure 7. Note that, for $Ln^{III}H(oep)(tpp)$, the Ln−N(tpp) distances form a more symmetrical distribution, with a smaller DW factor, than protonated $Ln^{III}H(tpp)_2$ complexes. The widths of the distributions are in good agreement, and hence, obtained from the fitting procedure with the theoretical phases and amplitudes (FEFF6), the DW factors reproduce well at low temperature the static distribution of the distances (the antiprism is distorted). Moreover, a small increase of the DW factors at room temperature is due to the increase of thermal motions.

$Ln^{III}H(tpp)_2$. As it was mentioned earlier,[15,16] all attempts to obtain crystals suitable for an XRD study for this kind of symmetrical dimer and whatever is the rare earth concerned have failed so far. Therefore XAFS analysis gives for the first time the structural parameters for these complexes. The one-shell fitting procedures give an unreasonable coordination number (six) for gadolinium as well as for samarium ions. The gadolinium ion is strongly bonded to the six nitrogen atoms at R(Gd−N_{av}) 2.51 Å with a small DW factor. The DW factor increases with temperature from 0.006 to 0.008 Å^2. The samarium ion is bonded to the six nitrogen atoms at the distance R(Sm−N_{av}) 2.53 Å with the DW factor 0.006 Å^2 at room temperature. Here we also introduce the two-shell model to take into account the strong asymmetry of RDF (presence of two nitrogen atoms at about 2.65 Å). The model matches the experimental signal better than the one-shell model and has a reasonable coordination number in agreement with the structure of bisporphyrinates.

Conclusions

Our XAFS analysis gives consistent structural information about the poor crystalline symmetrical Gd and Sm complexes. The XANES spectra of studied complexes are in good agreement with the expected Ln^{+3} oxidation state.

The XAFS results show that we were particularly sensitive to the decreasing amplitude of the signals and light changes in the first coordination sphere bonding mainly due to the protonation but also to a contribution of steric effects. For the

Ln−nitrogen first-shell coordination, the fit was done using both experimental and theoretical (FEFF) amplitudes and phases of the photoelectron.

The fitted parameters were gathered by calculating the RDFs, and we observed a longer bonding effect for the protonated $Ln^{III}H(oep)(tpp)$ and $Ln^{III}H(tpp)_2$ compounds, revealing a pronounced asymmetry with the displacement of the curves toward large distances. In contrast, the RDF of the nonprotonated complex $Ln^{III}(oep)_2$ presents a Gaussian form. Nevertheless it was important to take care of disorder effects especially with $Ln^{III}H(tpp)_2$ (lowest amplitude of the signal, highest DW factors) for which the substituents may cause a large deformation of the ring. Concerning this family of $Ln^{III}H(tpp)_2$ complexes, the structural data presented here are original as no crystalline form had been obtained previously.

The MS analysis of the carbon atom peaks (C_1 and C_2) confirms the dominance of the SS signals generated by the sixteen C_α and eight C_μ carbon atoms. The fitting results show that for gadolinium and respectively for samarium complexes the two-atom distribution ($Gd-C_\alpha$ and $Gd-C_\mu$) remains the same with the average distances $R(Gd-C_\alpha)=3.46 \pm 0.03$ Å and $R(Gd-C_\mu)=3.78 \pm 0.03$ Å.

Considering the signatures observed beyond the first three shells, strong MS contributions within near linear $Gd-N-C_\beta$ chains are generated (peak D). We have reached the limits of the XAFS technique concerning the difficulty to include, while calculating theoretical amplitudes and phases, the atoms far from the absorbing one beyond 5 Å, in particular the ligands ethyl and phenyl. Therefore we will develop in the near future the MS calculations and analysis on these crowded macrocyclic complexes.

Acknowledgment. This research was supported by the Greek General Secretariat of Research and Technology. J.P. would like to thank the Laboratoire de Chimie Bioinorganique—Centre pharmaceutique Châtenay-Malabry Université Paris-Sud, for their hospitality during this work. We also gratefully acknowledge the LURE laboratory.

Supporting Information Available: Figure S1 (XAFS spectra) and Figure S2 (FTs XAFS), showing the comparison of the MS calculations (the cluster of 32 and 48 atoms around the Gd) and experimental XAFS signals for the GdH(oep)(tpp) complex. Table S.1, showing the first coordination shell best-fit analysis with the theoretical phase and amplitude label (feff) including the asymmetry of RDF (C_3 cumulant). This material is available free of charge via the Internet at http://pubs.acs.org.

IC000410O